JOURNAL OF SOLID STATE CHEMISTRY **127,** 240–247 (1996)
ARTICLE NO. 0380

Boron Incorporation into Rutile. Phase Equilibria and Structure Considerations

Ian E. Grey,[1] Christina Li, and Colin M. MacRae

CSIRO Division of Minerals, Victoria, Australia

and

Les A. Bursill

School of Physics, Melbourne University, Parkville, Australia 3168

Received May 3, 1996; in revised form September 5, 1996; accepted September 6, 1996

Reduction of rutile in the presence of borate flux stabilizes the rutile phase relative to reduced rutiles due to incorporation of boron from the flux. In the presence of borates the rutile phase is stabilized to oxygen fugacities that are lower by almost two orders of magnitude compared with fugacities at the limit of the single-phase rutile phase field in the pure Ti–O system. Boron incorporation is accompanied by reduction of titanium to the trivalent state, according to the charge compensation relation: $3Ti^{4+} = 3Ti^{3+} + B^{3+}$ (interstitial). Results of powder X-ray diffraction and transmission electron microscopy studies on samples prepared in the temperature range from 1100 to 1300°C have been used to establish a model for boron incorporation. It is proposed that at the temperatures studied, local defects in boron-doped rutile form from displacement of titanium atoms to adjacent interstitial sites coupled with occupation by boron of the triangular face of the vacated octahedral sites. This atomic grouping represents a small element of the $TiBO_3$ (calcite-type) structure. Annealing at a lower temperature results in ordering of the local defects to form $(101)_r$ planar intergrowths of rutile and calcite-type structures.

INTRODUCTION

The use of borate fluxes in conjunction with controlled gaseous buffers to grow crystals of nonstoichiometric rutile and reduced rutile phases was first reported by W. B. White and colleagues in the 1960s (1, 2). At the time there was considerable interest in producing high quality single crystals for characterization of the magnetic and electrical properties of the reduced rutiles. An important consideration was thus the selection of a flux that did not impart impurities to the crystals during their growth. However analyses of the rutile crystals showed concentrations of boron which, although very low (<0.1 wt% B), could have influenced the electrical properties. The amount of boron in the crystals was observed to increase with decreasing oxygen fugacity of the gaseous atmosphere, from about 100 ppm for reactions in air to more than 800 ppm at an oxygen fugacity of $10^{-12.8}$ atm (at 1200°C). It was suggested that boron could be located at tetrahedral interstitial sites in the rutile structure, although no structural evidence was presented (1).

In the studies reported here we have investigated the uptake of boron from borate fluxes into rutile and reduced rutile phase as a function of temperature and oxygen fugacity. Powder X-ray diffraction (PXRD) and transmission electron microscopy (TEM) techniques have been applied to gain insight on the structural mechanism for boron incorporation.

EXPERIMENTAL

Mixtures of titanium dioxide (Aldrich 99.9+%, anatase form) and calcium borate, $Ca_2B_6O_{11} \cdot 5H_2O$ (4:1 weight ratio), were ground together, pelleted, and contained in a molybdenum boat. The samples were heated in a platinum wound tube furnace in reducing atmospheres obtained using mixtures of CO and CO_2. Reduction times were typically 6 to 16 h at temperatures in the range from 1100 to 1300°C. All samples were reground and reheated at least once. The attainment of equilibrium was checked by including pellets of reduced titanium oxide (Ti_6O_{11}) mixed with flux, and pellets of pure titania. The products from the reduction of the pure titania pellets were checked against

[1] To whom correspondence should be addressed.

[2] Since submitting the manuscript a laboratory relocation has been decided. The new address will be CSIRO Division of Minerals, Clayton, Victoria, Australia 3169.

0022-4596/96 $18.00

literature data. The product from one of the 1300°C fluxed preparations was leached in 2 *M* HCl to remove the borate flux, and then dried and reheated in an evacuated, sealed silica tube for 20 h at 1000°C to check if lower temperature annealing caused any structural ordering.

The phases present in the reduced products were identified by PXRD using a Philips diffractometer fitted with a graphite monochromator in the diffracted beam and employing Cu$K\alpha$ radiation. The X-ray tube was operated at 40 kV and 40 mA with 1° divergence and scatter slits, a 0.2 mm receiving slit, and soller slits in the incident and diffracted beams. Intensity measurements were made at intervals of 0.025° 2θ, using a step counting time of 0.5 sec for rapid-scan identification runs. For Rietveld refinements, variable counting time (VCT) data sets (3) were collected in the 2θ range from 20° to 140° using a total counting time of 30 ksec. Electron diffraction/microscopy studies were made using a JEOL-4000EX high resolution transmission electron microscope operated at 400 kV. Studies were made on thin edges of crystals produced by fracturing and on ion-beam thinned specimens. Individual crystals were also examined in a JEOL In-Lens-Field-Emission Scanning Electron Microscopy (IFESEM), capable of a resolution of 10 Å.

Least-squares structure refinements were carried out using the Rietveld program CSRIET, a local modification of the code by Hill and Howard (4) and Wiles and Young (5) that takes account of VCT data sets. Profile refinement parameters included a scale factor, a pseudo-Voigt peak shape parameter, a peak full-width at half maximum (FWHM) function (6) of the form $\mathrm{FWHM}^2 = U\tan^2\theta + V\tan\theta + W$, a 2θ zero parameter, and the unit cell parameters. The background was refined using a four-parameter polynomial in $2\theta^n$, $n = 0$–3. X-ray scattering factors for ionized atoms were used.

Chemical analyses were carried out on single-phase (by PXRD) titanate samples after leaching the crushed reaction pellets in 2 *M* HCl for 30 min at 60°C to remove the borate flux. A portion of the washed and dried leach residue was fused in sodium carbonate at 900°C, the fusion cake was dissolved in dilute nitric acid, and boron and calcium were analyzed in the solution by ICP. The extent of reduction (Ti^{3+} content) was determined from the weight gain on oxidizing the reduced samples in air at 900°C. Care had to be taken to avoid prolonged heating because of B_2O_3 volatilization. The boron content of individual rutile crystals was obtained by wavelength dispersive electron microprobe analysis, using a JEOL Superprobe microanalyzer, model JXA-8900R. The analytical procedure involved measuring the integrated area under the boron peak. Pure boron was used as a standard. The influence of the titania matrix was corrected by using measurements on boron-free rutile standard (are melted Aldrich 99.99% TiO_2). The microprobe results were typically averaged over 30 point analyses for each sample.

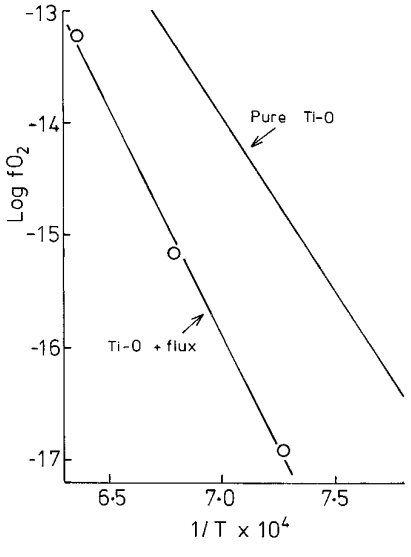

FIG. 1. Lower oxygen fugacity stability limits for pure and fluxed rutile, plotted as log fO_2 vs $1/T$, T in °K.

RESULTS AND DISCUSSION

Phase Equilibria

The borate flux was observed to have a controlling effect on the phase equilibria in the Ti–O system. In the presence of the flux the rutile phase was stabilized to lower oxygen fugacities than the pure Ti–O system. At each temperature studied in the phase equilibria experiments the oxygen fugacity was progressively lowered in successive runs until the PXRD pattern of the product showed the presence of some reduced rutile. The run for which the first trace of reduced rutile was distinguishable in the reduction product was taken to represent the lower fugacity limit of the rutile phase in the titania–flux system.

The log fO_2 values corresponding to the limit of the rutile field at different temperatures are plotted against $1/T$ in Fig. 1. The rutile phase boundary for the pure Ti–O system is shown for comparison, based on published results (7–9). It is seen from Fig. 1 that in the presence of the borate flux the oxygen fugacity at the rutile phase boundary is lowered by almost two orders of magnitude. In the pure Ti–O system, rutile at the single phase boundary is slightly nonstoichiometric with a composition close to $TiO_{1.992}$ (7). At lower oxygen fugacities the two-phase field, rutile + $TiO_{1.98}$, is stable (7), where $TiO_{1.98}$ is the upper composition limit of the homologous series of $(132)_r$ crystallographic shear (*CS*) structures (7). However in the presence of borate flux, reduction at fugacities below the rutile single phase field gives two phase mixtures of rutile + $TiO_{1.875}$,

TABLE 1
Characterization of Single Phase Boron-Doped Rutile Products

Temperature (°C)	log fO_2 (atm)	B content (wt%)	Ti^{3+} content (wt%)	[Ti]/[B] atom ratio	Cell parameters (Å)	
					a	*c*
1100	−15.0	0.15	2.0	3.0	4.6005(1)	2.9624(1)
1100	−15.8	0.25	2.2	2.0	4.6029(1)	2.9635(1)
1100	−17.0	0.32	4.7	3.3	4.6067(1)	2.9659(1)
1200	−15.2	0.34	5.0	3.3	4.6078(1)	2.9666(1)
1300	−13.3	0.33	4.8	3.3	4.6077(1)	2.9665(1)
1000 anneal	sealed tube	0.29	na		4.6078(1)	2.9666(1)

where $TiO_{1.875} \cong Ti_8O_{15}$ is the highest *n*-even homolog of the Ti_nO_{2n-1} family of $(121)_r$ *CS* phases (7).

The approach to equilibrium by oxidation of Ti_6O_{11}/flux mixtures was observed to be extremely slow. Samples equilibrated at oxygen fugacities within the rutile phase field gave mixtures of Ti_8O_{15} and a small amount of rutile. Successive grinding and reheating resulted in a gradual increase in the amount of rutile relative to Ti_8O_{15}, but even after 3 or 4 reheats some Ti_8O_{15} persisted. The difficulty in achieving equilibrium appears to be a consequence of very slow kinetics of oxygen exchange through the flux when CO/CO_2 is used as the gaseous buffer. A test was made using a H_2/CO_2 gas mixture and a higher rate of exchange was observed. Despite the better reaction kinetics, H_2/CO_2 buffers were not used for the present study because the presence of water vapor leads to relatively rapid volatilization of boron from the flux as gaseous H_3BO_3 and HBO_2.

The product from the 1300°C equilibration at the lower oxygen fugacity limit of the rutile phase field was leached in 2*M* HCl to remove unreacted flux and then was dried, pressed into a pellet, and sealed in an evacuated silica tube. It was heated overnight at 1000°C in an attempt to order the contained boron as a separate phase. A PXRD pattern of the annealed product showed a minor amount of Ti_8O_{15}, in addition to rutile. This sample was used for the transmission electron microscope studies as described below.

Rutile Composition

By analogy with the study by Berkes *et al.* (1) the phase obtained at the lower fugacity limit of the rutile phase field should contain the maximum boron content. Accordingly these products at each temperature were subjected to detailed analyses. The results of chemical analyses and unit cell parameter refinements are reported in Table 1. Also included in Table 1 are analyses of samples equilibrated at higher fugacities within the rutile phase field at 1100°C.

The analyses for trivalent titanium and boron contents in the limiting rutile compositions give atomic ratios of [Ti]/[B] close to 3. This suggests a charge-compensating substitution mechanism for incorporating Ti^{3+} into rutile in the presence of boron,

$$3Ti^{4+} \leftrightarrow 3\ Ti^{3+} + B^{3+}(\text{interstitial}),$$

i.e., three Ti^{3+} ions replacing three Ti^{4+} ions, with charge compensation being maintained by incorporation of boron into suitable interstitial sites.

The maximum boron content in rutile under reducing conditions is about 0.33 wt% B and is relatively independent of the reduction temperature. Using this figure and a [Ti/]/[B] atomic ratio of 3 the rutile composition is calculated to be $[Ti^{4+}_{0.928}Ti^{3+}_{0.072}B_{0.024}]O_2$. In agreement with previous work (1, 2) we find that the boron incorporation decreases with increasing oxygen fugacity. As seen from Table 1, at 1100°C the boron level in rutile is halved when fO_2 is increased from 10^{-17} to 10^{-15} atm.

In contrast to the significant boron levels in rutile under reducing conditions, much lower levels of boron were incorporated into reduced rutile phases. For example, microprobe analysis of reduced rutile from a fluxed reduction carried out at an oxygen fugacity below the stability field for rutile gave only 0.02 wt% B. This is consistent with the work of Bartholomew and White, who reported levels of 0.014–0.015 wt% B in Ti_3O_5 and Ti_4O_7 (2).

PXRD and EM Studies

A general observation was that the PXRD patterns of rutile phases prepared in the presence of borate flux showed severe preferred orientation, with strong enhancement of the intensities of the $\{hh0\}_r$ reflections. The preferred orientation was enhanced by ball milling and micronization techniques used for PXRD sample preparation. The origin of the preferred orientation was the flux-induced growth of rutile in the form of thin platelets. These were identified from an IFESEM examination of individual fluxed rutile crystals. Typical IFESEM photomicrographs

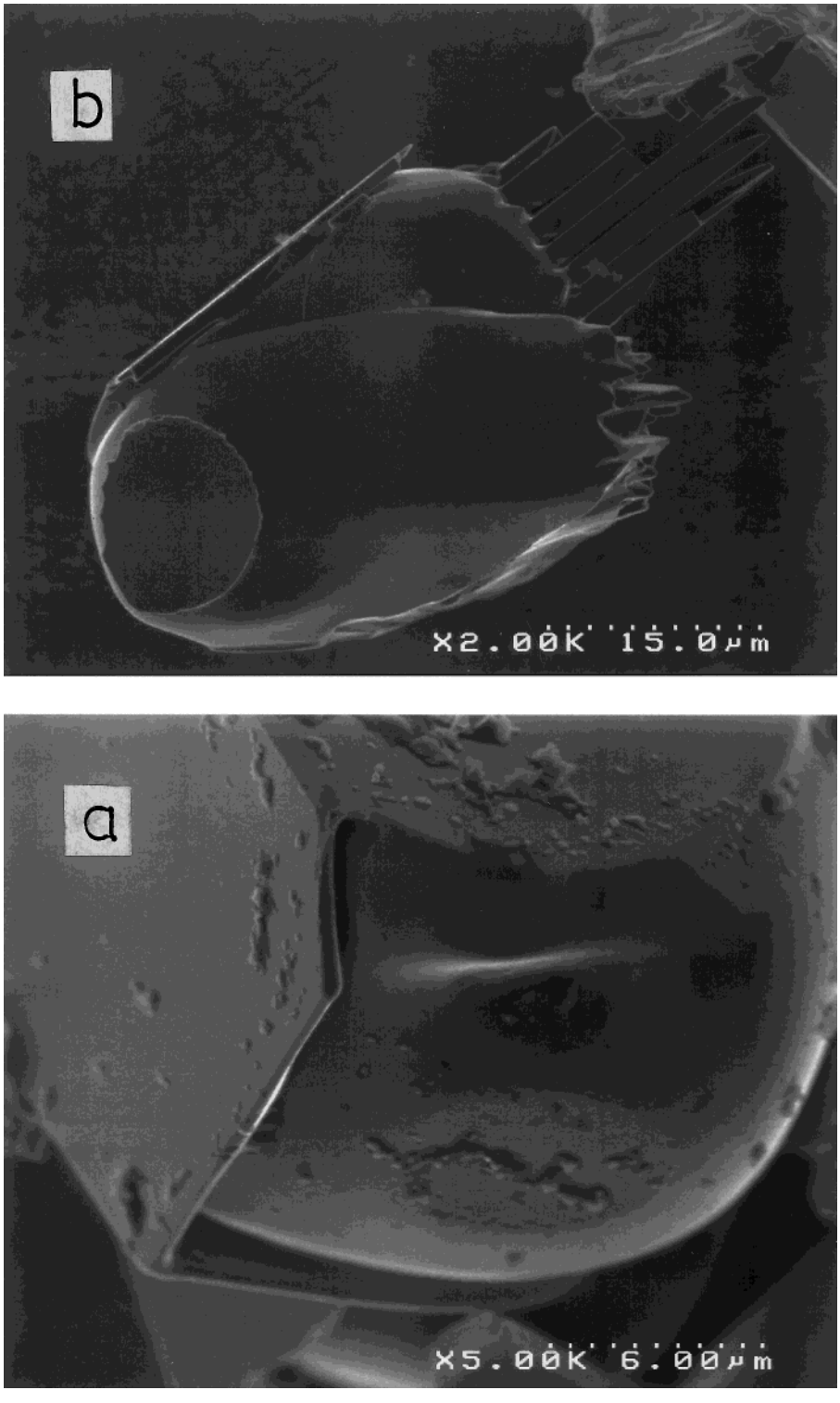

FIG. 2. IFESEM photomicrographs showing platelike extensions of rutile crystals grown in borate flux.

are shown in Fig. 2. The rutile crystals were generally in the form of rounded anhedral grains, but the majority of them were encompassed in box-like ''tubes'' formed by thin platelets fused together at right angles. This is illustrated in the photomicrograph in Fig. 2a. Another common occurrence was the growth of very thin plate ''finger-like'' crystals from the main crystal body, as shown in Fig. 2b. On crushing or grinding, these platey appendages would

TABLE 2
Summary of VCT Rietveld Refinements of Rutile and B-Doped Rutile (1300°C, $fO_2 = 10^{-13.5}$ atm)

	Rutile	B-doped rutile
Cell parameters (Å)		
a	4.5940(1)	4.6092(1)
c	2.9589(2)	2.9673(1)
Oxygen *x* coord. (*xx*0)	0.3047(2)	0.3042(2)
Thermal parameters (Å^2)		
B(Ti)	0.42(1)	0.73(1)
B(O)	0.30(2)	0.36(2)
R_{wp}	11.8	13.9
R_B	3.7	9.1
GOF	2.6	5.1
Preferred orientation	None	(110) POP = 0.82

be released and confer preferred orientation on the powder samples. The PXRD patterns are consistent with $\{hh0\}_r$ habits for the plate-like crystals.

The results of VCT Rietveld refinement of rutile with maximum boron content (prepared at 1300°C, see Table 1) are summarized in Table 2. For comparison, the results are given for pure rutile (Aldrich 99.99% TiO_2 heated to 900°C), using identical data collection and refinement procedures. The main change to the boron—doped rutile is an expansion of the unit cell, with increases of 0.3 and 0.4% for the *a* and *c* axes, respectively, relative to pure rutile. The thermal parameters are larger for the boron doped rutile and the *R* factors are considerably higher. A difference Fourier map showed that the main residual electron density occurred at (1/2 0 0) and related positions, corresponding to the empty octahedral sites in the $(001)_r$ channels in rutile. However, inclusion of an atom at this site and refinement of its occupation factor did not result in a significant improvement in the agreement factors.

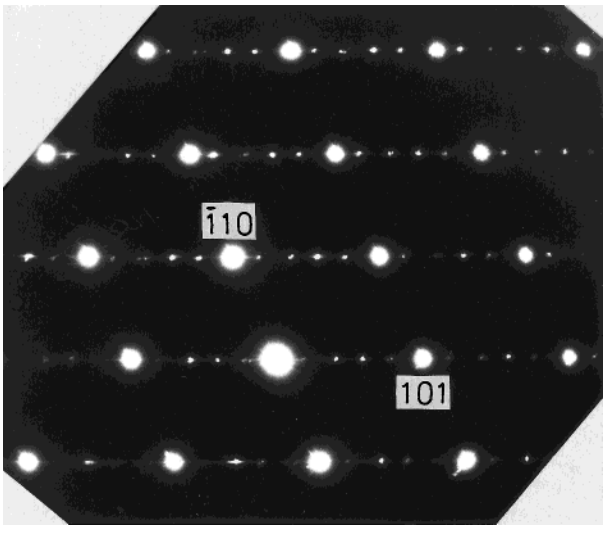

FIG. 4. $[11\text{-}1]_r$ zone axis electron diffraction pattern of boron-doped rutile annealed at 1000°C, showing 5× superlattice spots along $\mathbf{k}_{101}$.

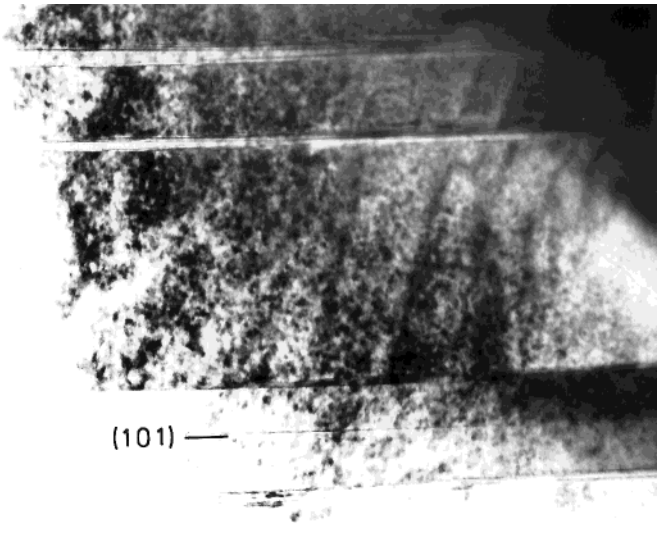

FIG. 3. TEM image from boron-doped rutile crystals showing extensive mottling due to local defect clusters, as well as $(101)_r$ twin boundaries.

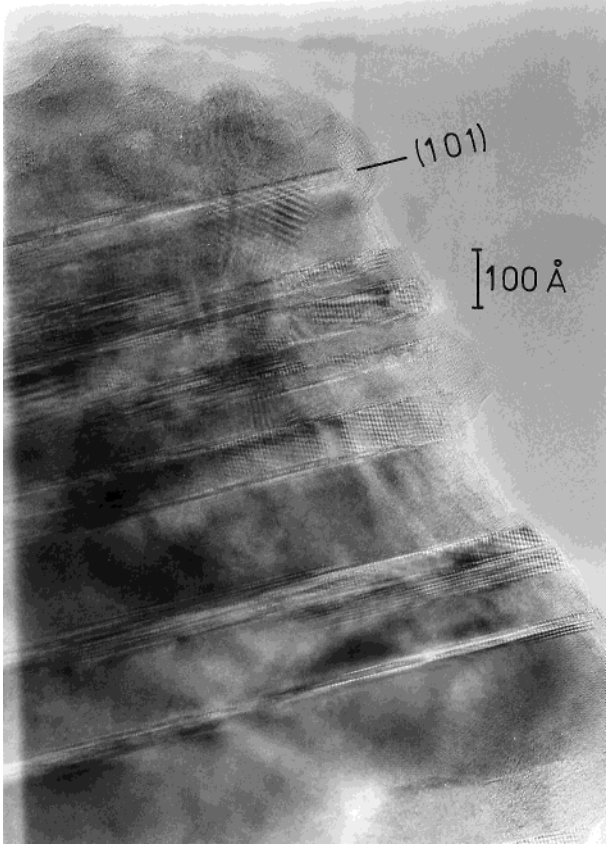

FIG. 5. TEM image corresponding to the diffraction pattern in Fig. 4.

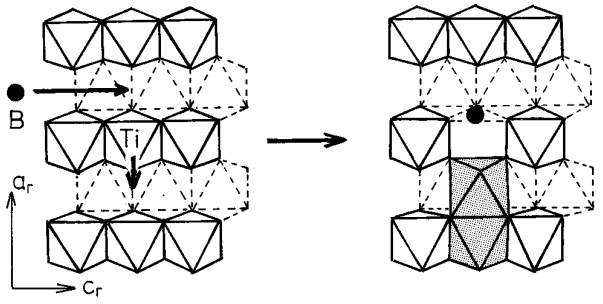

FIG. 6. Model for boron incorporation into rutile. Boron (filled circle) occupies a triangular face of a vacated octahedron. Displaced titanium atom moves to interstitial octahedral site which shares a face with a second octahedron. Face-shared octahedra (shaded) and boron atom form a $[100]_r$ linear defect cluster.

Unit cell parameters obtained by Rietveld refinement of the various boron-doped rutile samples are reported in Table 1. Both the a_r and c_r parameters show a linear dependence on boron content of the rutile, given by a_r (Å) = 4.594 + 0.040 (wt%B), c_r (Å) = 2.959 + 0.022 (wt%B); the largest deviation between observed and calculated parameters is 0.001 Å.

Transmission electron microscope images from boron-doped rutile crystals showed no evidence of extended planar defects, platelets, or other forms that would indicate ordering and separation of boron-containing phases. The only planar boundaries observed were $\{101\}_r$ microtwins, which are the most common forms of release of mechanical strain in rutile. $[11\text{-}1]_r$ zone axis diffraction patterns (DPs) showed twinned reflections and weak streaks along $\mathbf{k}_{101}$. Electron energy loss spectroscopy was used to analyze for boron in the vicinity of the microtwin boundaries. No evidence was obtained for increased concentrations of boron at these boundaries.

Although no extended defects were observed, the images consistently showed fine-scale spot contrast (mottling) that was not present in undoped rutile crystals. An example is shown in Fig. 3. This type of spot contrast has been previously noted in TEM images of chromia-doped rutiles (10) and its presence has been explained in terms of the formation of small defect clusters.

The $[11\text{-}1]_r$ zone axis DPs for the 1000°C annealed sample showed the development of superlattice spots along $\mathbf{k}_{101}$ with a separation of approximately 1/5 $\mathbf{k}_{101}$, as shown in Fig. 4. The corresponding image, Fig. 5, shows groupings of relatively poorly ordered planar boundaries parallel to $(101)_r$ with a periodicity of about $5 \times d(101)_r \sim 12$ Å.

Models for Boron Incorporation

The absence of extended defects in the TEM images suggests that the boron is incorporated coherently into the rutile structure. The analytical data is consistent with a coupled substitution of boron with trivalent titanium. Berkes *et al.* (1) suggested that boron could be located at tetrahedral sites in the rutile structure. However, charge balance calculations suggest that this is not very likely. Each oxygen anion in rutile is coordinated to 3 titanium cations. Allowing for 3 Ti^{3+} ions per B^{3+}, the formal valence sum at oxygen sites tetrahedrally coordinated by boron is 2.625, corresponding to severe oversaturation. If the boron is in triangular rather than tetrahedral coordination the valence sum is worse at 2.875.

The problem of anion valence oversaturation can be resolved if we allow boron incorporation to be accompanied by titanium diffusion from an occupied octahedral site to an adjacent empty octahedral site in the $[001]_r$ channels. This is illustrated in Fig. 6. A titanium atom is displaced by 1/2 $[100]_r$ through an octahedral face into the adjacent octahedral site, producing a pair of face-shared cation-centered octahedra. The empty octahedron produced by this migration now has a triangular face in which the anions are only two-coordinated by titanium atoms. The boron atom is incorporated into rutile at this triangular face as shown in Fig. 6. Allowance for three trivalent titanium atoms per boron atom (two of these would have a high probability of being ordered into the face-shared octahedra) gives valence sums close to 2 for the anions involved in the defect cluster. This local defect model is closely related to the linear cationic interstitial model developed to explain Cr^{3+} incorporation into rutile (11). In the latter case, incorporation of Cr^{3+} into an interstitial octahedral site in rutile is accompanied by diffusion of

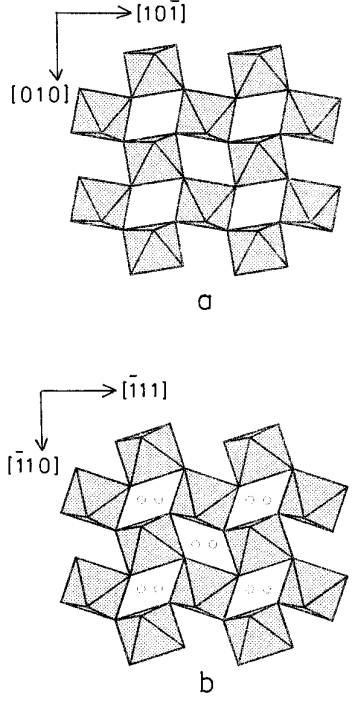

FIG. 7. Equivalent atomic arrangements in (a) $(101)_r$ rutile layer and (b) $(1\text{-}12)_c$ calcite layer (open circles are carbon atoms).

TABLE 3
Equivalent Atomic Layers in TiO_2 and $TiBO_3$ Structures

	TiO2	$TiBO_3$
Structure type	rutile	calcite
Symmetry, cell	tetragonal, $P4_2/mnm$	trigonal, $R\text{-}3c$
	a = 4.5937 Å, c = 2.9587 Å	a = 4.6723 Å, c = 14.949 Å
Volume per oxygen (Å^3)	15.6	15.6
Related layers of corner-linked octahedra	{101}	{1–12}
Orthogonal dimensions in above layers	[10-1] = 5.46 Å [010] = 4.59 Å	1/3[−111] = 5.65 Å [−110] = 4.67 Å

titanium from an occupied to an adjacent empty octahedral site, giving a linear $[100]_r$ grouping of two pairs of face-sharing octahedra.

The topology of the boron-centered cluster resembles a small fragment of the calcite structure, which is adopted by the trivalent titanium borate, $TiBO_3$ (12). The rutile and calcite structures are in fact closely related, the $\{100\}_r$ planes in rutile being topologically identical to the $\{1\text{-}12\}_c$ calcite planes. This is illustrated in Fig. 7, where the relevant planes in the two structures are compared. In a formal sense the rutile structure can be derived from the calcite structure by periodic crystallographic shear, on $\{1\text{-}12\}_c$, of the corner-linked octahedral MO_3 framework (13).

There is a close dimensional match of the atomic arrangements in the $\{101\}_r$ planes in TiO_2 and the $\{1\text{-}12\}_c$ planes in $TiBO_3$ as shown by the data in Table 3. This suggests that agglomeration of boron-centered defect clusters of the type shown in Fig. 6 could occur on these planes. Ultimately, extended planar defects could form, based on intergrowth of rutile and calcite structures. Such an ordered intergrowth of the two structure types has been reported for the high pressure phase of niobium oxide, B-Nb_2O_5 (14). The latter phase has monoclinic symmetry. $C2/c$, with $a \sim 2a_r + 3c_r$ = 12.73 Å, $b \sim b_r$ = 4.88 Å, $c \sim -a_r + c_r$ + 5.56 Å, β = 105.05°. A projection of the structure along **b** is shown in Fig. 8. The repeat distance perpendicular to $(100) = (101)_r$ is approximately $5 \times d(101)_r$. This is consistent with the superstructure observed in ED patterns of annealed boron-doped rutile (Fig. 4). The contrast seen in magnified regions of the corresponding image, Fig. 5, matches with the projected metal atom distribution of the intergrowth structure. It thus appears that unit cell intergrowth of TiO_2 and $TiBO_3$ occurs in annealed boron-doped rutiles prepared under reducing conditions, although as seen from Fig. 5, the extension of the intergrowth structure perpendicular to $(101)_r$ is limited to a few tens of angstroms only.

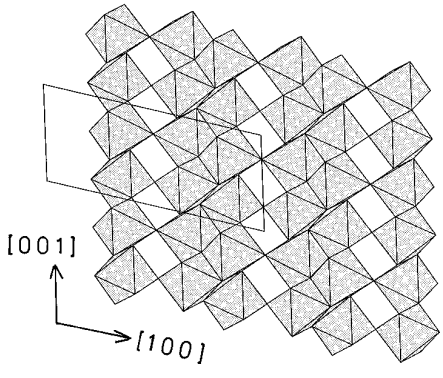

FIG. 8. Projection of structure for B-Nb_2O_5 along [010]. This is the structure proposed for intergrowth of TiO_2 and $TiBO_3$ in annealed boron-doped rutile.

SUMMARY

In summary, under reducing conditions, boron is incorporated into the rutile structure. The boron incorporation requires partial reduction of titanium to the trivalent state according to the charge-coupling substitution reaction: $3Ti^{4+} \leftrightarrow 3\ Ti^{3+} + B^{3+}$ (interstitial). In the presence of boron the rutile phase is stabilized to oxygen fugacities two orders of magnitude lower than in the pure Ti–O system. The amount of incorporated boron increases with decreasing oxygen fugacity and attains a maximum value of about 0.33 wt% B at the lower fO_2 phase boundary. This value is essentially independent of temperature. The majority of the boron is incorporated as local defect clusters which are manifested in electron microscope images as mottled spot contrast. A model for a defect cluster is presented which involves boron in threefold coordination to anions forming a triangular face of an empty octahedron, associated with a pair of occupied face-shared octahedra. The BO_3 triangles and the face-shared octahedra form linear defects along $\langle 100 \rangle_r$. Evidence is presented for the agglomeration of local defect clusters into extended structures involving ordered unit cell intergrowth of planar TiO_2 and $TiBO_3$ (calcite-type) structure elements, parallel to $(101)_r$.

REFERENCES

1. J. S. Berkes, W. B. White, and R. Roy, *J. Appl. Phys.* **36,** 3276 (1965).
2. R. F. Bartholomew and W. B. White, *J. Crystal Growth* **6,** 249 (1970).
3. I. C. Madsen and R. J. Hill, *Adv. X-Ray Anal.* **35,** 39 (1992).
4. R. J. Hill and C. J. Howard, *J. Appl. Crystallogr.* **18,** 173 (1985).
5. D. B. Wiles and R. A. Young, *J. Appl. Crystallogr.* **14,** 149 (1981).
6. G. Caglioti, A. Paoletti, and F. P. Ricci, *Nucl. Instrum.* **3,** 223 (1958).
7. R. R. Merritt, B. G. Hyde, L. A. Bursill, and D. K. Philp, *Phil. Trans.* **274,** 627 (1973).
8. P. Kofstad, *J. Phys. Chem. Solids* **23,** 1579 (1962).
9. K. S. Forland, *Acta Chem. Scand.* **18,** 1267 (1964).
10. L. A. Bursill, D. J. Smith, and Peng Ju Lin, *J. Solid State Chem.* **56,** 203 (1985).
11. L. A. Bursill, M. G. Blanchin, and D. J. Smith, *Philos. Mag. A.* **50**(4), 453 (1984).
12. M. Huber and H. J. Deiseroth, *Z. Krist.* **210,** 685 (1995).
13. S. Andersson and J. Galy, *J. Solid State Chem.* **1,** 576 (1970).
14. F. Laves, W. Petter, and H. Wulf, *Naturwiss.* **51,** 633 (1964).